Article

Neuro-Fuzzy Based High-Voltage DC Model to Optimize Frequency Stability of an Offshore Wind Farm

Muhammad Shoaib Bhutta [1], Tang Xuebang [1,*], Muhammad Faheem [2,*], Fahad M. Almasoudi [3], Khaled Saleem S. Alatawi [3] and Huali Guo [1]

1   School of Automobile Engineering, Guilin University of Aerospace Technology, Guilin 541004, China;
    shoaib@guat.edu.cn (M.S.B.); guohuali@guat.edu.cn (H.G.)
2   Department of Computing Technology and Innovations, University of Vaasa, 65200 Vaasa, Finland
3   Department of Electrical Engineering, Faculty of Engineering, University of Tabuk,
    Tabuk 47913, Saudi Arabia; falmasoudi@ut.edu.sa (F.M.A.); khaled@ut.edu.sa (K.S.S.A.)
*   Correspondence: tangxb@guat.edu.cn (T.X.); muhammad.faheem@uwasa.fi (M.F.)

Abstract: Lack of synchronization between high voltage DC systems linking offshore wind farms and the onshore grid is a natural consequence owing to the stochastic nature of wind energy. The poor synchronization results in increased system disturbances, grid contingencies, power loss, and frequency instability. Emphasizing frequency stability analysis, this research investigates a dynamic coordination control technique for a Double Fed Induction Generator (DFIG) consisting of OWFs integrated with a hybrid multi-terminal HVDC (MTDC) system. Line commutated converters (LCC) and voltage source converters (VSC) are used in the suggested control method in order to ensure frequency stability. The adaptive neuro-fuzzy inference approach is used to accurately predict wind speed in order to further improve frequency stability. The proposed HVDC system can integrate multiple distributed OWFs with the onshore grid system, and the control strategy is designed based on this concept. In order to ensure the transient stability of the HVDC system, the DFIG-based OWF is regulated by a rotor side controller (RSC) and a grid side controller (GSC) at the grid side using a STATCOM. The devised HVDC (MTDC) is simulated in MATLAB/SIMULINK, and the performance is evaluated in terms of different parameters, such as frequency, wind power, rotor and stator side current, torque, speed, and power. Experimental results are compared to a conventional optimal power flow (OPF) model to validate the performance.

Keywords: frequency stability; hybrid HVDC system; line commutated converter; neuro-fuzzy controller; voltage source converter; offshore wind farm

1. Introduction

The production of wind energy is regarded as the leading renewable energy source because of its reliability, stability, and efficient power generation. In comparison to onshore wind farms, the wind speed in offshore wind farms (OWFs) is potentially higher and more stable, which contributes to increased power generation. There are also few restrictions on the implementation of OWFs compared to onshore wind farms [1–4]. It is anticipated that the generation of wind energy using OWFs can be nearly 54 GW in the United States [5]. The technical complexities associated with the implementation of offshore platforms and the process of transferring power from OWF to onshore power grids needs significant attention [6–8]. Previous studies have shown that the HVDC transmission is superior to HVAC transmission in terms of improved technical and economic feasibility, sustainability, and flexibility of integration with larger wind farms located at greater distances [9,10]. Researchers have investigated the application of HVDC systems which utilize voltage source converters (VSC) [11,12] and line commutated converters (LCC) [13,14] for integrating OWFs. Compared to LCC based power transmission, VSC based systems offer better advantages in terms of fast response and better control. HVDC systems with VSC

do not require any external voltage source, and they are independent of active or reactive power controls [15]. The concept of an offshore wind generating system that combines the benefits of VSC and LCC in a hybrid multi-terminal HVDC (MTDC) system is gaining popularity [16]. In these systems, VSC is used to connect with the OWF without using any communication source, and LCCs are placed near the onshore electrical grid in order to reduce the energy losses and reduce installation costs.

The work presented in [17] suggested a wind speed correction method based on a modified HMM (hidden Markov model) that effectively enhanced the accuracy of wind power forecasts. The incorporation of historical wind speed patterns through the modified HMM enabled the model to capture complex dynamics and to improve the precision of wind power predictions. Furthermore, [18] proposed a compensation strategy for wideband voltage harmonics in DFIG-based wind energy conversion systems. The strategy combined harmonic detection using a modified SRF-PLL and compensation through a cascaded control structure. The results demonstrated the successful mitigation of harmonics, leading to improved power quality and enhanced performance of the DFIG. The research in [19] introduced a low-pass virtual filter as an effective method for smoothing the output power of wind energy conversion systems. The filter dynamically adjusted the power output based on the rate of change in wind speed, resulting in a more consistent power profile. The proposed approach offers potential benefits for the integration of wind energy into the power grid, improving system stability and reliability.

The work in [20] demonstrated an approach to construct simplified models for the dynamic analysis of monopile-supported offshore wind turbines. The proposed models generated a balance between accuracy and computational efficiency, allowing for efficient analysis and optimization of OWT designs. The work presented in [21] also proposed a novel output feedback control design methodology for fixed-time stabilization of high-order uncertain nonlinear systems. The proposed control approach, which is based on backstepping, guarantees stability within a specified timeframe. Additionally, the settling time analysis provides a quantitative measure of system performance.

Several pieces of research have addressed the implementation of a hybrid MTDC system to integrate wind farms. In [22], a hybrid MTDC system was suggested, with one side of the grid employing LCC and the other containing a VSC. However, the flexibility of this system was reduced due to poor operational flexibility. A five-terminal hybrid MTDC was proposed by [23]. The DC voltage of the MTDC in this system was regulated by a single converter, but the lack of controlling ability and the loss reduced the efficiency of this system. The flexibility of operating under different conditions was also not discussed. A hybrid system communicating with wind farms through a VSC based HVDC system was developed in [24]. Since LCC cannot reverse its direction, this method needs further exploration. With the rise in the adoption of HVDC systems for bulk power transmission, the complexities associated with hybrid HVDC systems, such as frequency regulation and stability, will also increase. Furthermore, the communication between HVDC systems in OWFs and onshore wind farms pose significant challenges with respect to operational stability and reliability [25–28]. This problem increases with the rise in the stochasticity of the wind speed, and, hence, it becomes difficult to control and stabilize the voltage and frequency of hybrid HVDC systems using conventional controllers. Various techniques have been proposed for improving the stability of the frequency and the voltage of hybrid HVDC systems [29–32]. However, the dynamic and stochastic behavior of the HVDC system increases the scope of research in this field. There is a need for an effective controlling strategy that can stabilize the frequency of HVDC systems in OWFs. The frequency stability problem is closely related to OWF integrated with grid connected systems. Additionally, the abbreviations used in this paper are presented at the end of the paper.

Review of Previous Works

Multi-terminal HVDC systems offer various benefits and contributes significantly in the integration of wind farms with power grids. However, maintaining frequency stability

in interconnected grid systems is a complex task. Various researchers have proposed different controlling strategies in order to address this problem [33–35]. The frequency stability problem is more complicated in asynchronously interconnected grids due to their inherently zero-inertia characteristics. In addition, large-scale power loss increases the demand for inertia in order to achieve frequency stability [36]. With the increasing implementation of RES with grid systems, a significant portion of traditional synchronous units are being replaced by non-synchronous RES, which increases the issues of frequency instability. Because of this, the frequency-related limitations are added into the system analysis in order to resolve this issue. The work proposed in [37–39] included governor rate and preventive security constraints in order to ensure stability after the sudden reduction in power generation.

Accordingly, research in [40,41] has examined how frequency constraints relating to power generation using renewable energy sources, notably wind energy, were affected by inertia response. As can be inferred from these works, most researchers have focused on controlling the under-frequency consequences caused by interrupted power generation. The effects of frequency consequences followed by the interruption of a HVDC link is the least focused. The fast response and the swift controllability of HVDC links strengthen the operational security of the grid systems. The work presented in [42] discussed the frequency control strategies in HVDC systems. The characteristics were analyzed based on the variations in the measurements of the system. The assessment of the MTDC system with respect to stability was reported in [43]. This work investigates the effect of voltage stability and factors influencing the potential efficacy of the system. The work also discusses the control techniques to deal with the issues that result in a complete shutdown of the system. Other research [44–47] is dedicated to the analysis of different control strategies for frequency stability enhancement. The authors introduce a novel approach for controlling T-S fuzzy wind turbine systems, utilizing an adaptive memory-event-triggered static output control technique. The main objective of the proposed method is to enhance the control performance of wind turbines by decreasing the computational complexity and the communication demands [48].

The lack of synchronization between high-voltage DC (HVDC) systems linking offshore wind farms and the onshore grid can have a significant impact on both the stability and the performance of the overall power system. There are some specific ways in which this lack of synchronization can affect the power system [49], and they are as follows. Frequency instability: If the offshore wind farms are unable to provide the required amount of power to the grid due to a lack of synchronization, this can lead to frequency fluctuations in the power system. This can cause instability in the system, and it could potentially lead to blackouts. Power loss: If the HVDC systems linking offshore wind farms and the onshore grid are not synchronized, it can lead to power losses due to inefficient transmission, which can result in a reduction in the overall power output of the wind farms and an increase in transmission losses. Grid contingencies: Lack of synchronization can lead to grid contingencies, such as voltage instability, overloading of transmission lines, and unbalanced power flows. These types of contingencies can destabilize the power system, and they can lead to equipment damage or failure [50].

However, there are certain drawbacks that can be inferred from these existing works, such as poor inertia and stability, increased power loss during the long-distance transmission of power, and difficulty managing the stochastic nature of wind power. To mitigate such problems, some innovative control techniques that integrate two methods, such as VSC–LCC, are implemented in order to achieve frequency stability in DFIG-based offshore wind farms.

This paper provides a comprehensive analysis of the frequency and the stability of multi-terminal HVDC systems for OWFs. The proposed approach is designed for analyzing the stability of HVDC systems for different wind speeds and loads. Since offshore wind farms are highly susceptible to the variation in the frequency stability, a STATCOM is employed in this research in order to increase the transient stability of the HVDC system.

STATCOM is also used to enhance the voltage regulation of the VSC and to maintain the voltage in phase with the system's voltage. Furthermore, this study employs an ANFIS (Adaptive Neuro-Fuzzy Inference System) based controller to optimize generating capacity by forecasting wind speed and to strengthen the system during fault occurrences. The main contributions of the proposed research are outlined in the points below:

i.   This research presents a coordination control strategy that combines LCC and VSC with a novel hybrid LCVSV-HVDC system for frequency stability analysis in DFIG based offshore wind farms.

ii.   This research focuses on improving the integration of off-shore wind farms using hybrid MT-HVDC for large-scale power transmission over long distances.

iii.   An ANFIS based controlling technique is used for forecasting the wind speed and to maximize the power generation.

The proposed control strategy offers several advantages over existing methods in terms of frequency stability, including the use of a hybrid LCVSV-HVDC system, improved integration of offshore wind farms, and an ANFIS-based controlling technique [51]. Moreover, the proposed control strategy is flexible and adaptable, and it caters to the ever-changing dynamics of both wind speed and power demand. This adaptability allows the system to maintain frequency stability under varying operating conditions, thereby ensuring a reliable power supply and minimizing the impact of disturbances on the overall grid [52].

The paper is organized further as follows: Section 2 presents the mathematical modeling of the HVDC system. Section 3 elaborates the control strategy used in this work. Section 4 briefly recounts the results of the simulation analysis, and Section 5 is the conclusion of the paper with the main observations and suggestions for future research.

2. Mathematical Modeling & System Configuration

The DFIG consisting of OWF with a 50 MVAR STATCOM is linked with a bus containing five wind turbines. In order to provide reactive power to the system as required, the STATCOM is connected to power inverters. A DFIG-based wind turbine (WT) powers the OWF, which operates at a variable speed through a gearbox. The mathematical modeling of HVDC components is discussed in this section.

2.1. Mathematical Model of the WT

The following steps describe the mathematical model of the WT: the rate of change of kinetic energy is used to determine the wind energy's power P, and, mathematically, it is expressed as [53]:

$$P = \frac{dE}{dt} = \frac{1}{2}\frac{dm}{dt}v_w^2 \tag{1}$$

Here, dm/dt is the mass flow rate, which is also expressed as $\rho A v_w$, and ρ presents air density and A represents area of wind. Equation (1) can be reduced as follows [53]:

$$P = \frac{1}{2}\rho A v_w^3 \tag{2}$$

The extracted mechanical power P_w from the wind turbine can be evaluated as the difference between the wind powers flowing upstream and downstream, and, mathematically, it is expressed as [53]:

$$P_w = \frac{1}{2}\rho A v_w \left(v_u^2 - v_d^2\right) \tag{3}$$

Here, v_u is the wind speed measured in meters per second (m/s) upstream at the rotor blades' initial point and v_d is downstream wind speed at the rotor blades' ends in m/s. The mechanical power is affected by various external and internal parameters, such as density,

power coefficient, and area. Considering these factors, the mechanical power expressed in Equation (3) can be modified as follows [53]:

$$P_w = 0.5 \times \rho \times C_P \times V^3 \times A \tag{4}$$

where P_w is the air flow's mechanical power in *watts* and C_P represents the power coefficient. The highest power that the WT can produce is estimated to be 50% or 0.5 times of the power that is available. The wind turbine's Tip Speed Ratio (*TSR*) is specified as follows [53]:

$$\lambda = \frac{(\Omega \times R)}{V} \tag{5}$$

Here, Ω denotes the mechanical velocity of the wind turbine at the rotor shaft in *rad/s*, R presents the radius of blade in *m*, and V represents the air velocity in m/s. The blade pitch angle β and the *TSR* values are utilized in order to determine the rotor power coefficient (C_P). The rotor power coefficient is expressed as [53]:

$$C_P = \left(\frac{Power\ Extracted}{Wind\ Power} \right) \tag{6}$$

Equation (4) can be modified as [53]:

$$P_w = 0.5 \times \rho \times C_P(\lambda,\ \beta) \times V^3 \times A \tag{7}$$

2.2. DFIG-Based OWF Model

The DFIG system in this research is implemented with an RSC controller at rotor side and a GSC controller at grid side. The DFIG system is coupled with the WT and the wind speed is varied, and the respective changes in the torque, the grid current, the stator current, and the power are observed. By means of a rotor-side converter (RSC), a grid-side converter (GSC), and a DC connection, the stator windings of the DFIG are linked to the step-up transformer's low-voltage side, and the rotor windings are connected to the same side. The RSC and the GSC connected across the input of the AC voltage govern the functioning of the DFIG system. The main objective of employing the RSC and the GSC is to concurrently regulate the active and reactive power of the grid. The RSC in a DFIG-based hybrid HVDC system regulates the rotor current across the d and q axis based on the stator flux-oriented control.

2.2.1. GSC Controller

The GSC in the DFIG is mainly utilized to control the voltage across the DC connection and to maintain the unity power factor throughout the operation. The GSC maintains the stability and the reliability of the multi-terminal HVDC systems, and it thereby maintains the power balance. The reactive current reference of the GSC is calculated using the following equation [54].

$$i_{q.GSC}^* = K_{iq} \left(V_{grid} - V_0 \right) \tag{8}$$

where K_{iq} is the reference value which is set as *2pu/$\triangle$V*, and *I*q* is the value of the reference current measured across the 'q' axis. The reference current is tracked using an internal control loop.

2.2.2. RSC Controller

The RSC controller allows the system to operate with unity power factor and to enhance the accuracy of the voltage regulation process. The current through the DFIG across the d-q axis denoted as ($i_{q,r,w}$, $i_{d,r,w}$) is determined by keeping the voltage and the active power across the stator winding at the specified values, respectively. In order to enable the wind turbines to generate desired frequency response, an external control loop

is added which causes an increment of inertia and damping into the system. Therefore, the modulation of frequency is determined as follows [54]:

$$P^*_{WT} = P_{WT} - K^f_{Droop}\Delta f_{WPP} - K^f_{inertia}\frac{d}{dt}\Delta f_{WPP} \tag{9}$$

where $K^f{}_{Droop}$ and $K^f{}_{inertia}$ are defined as the coefficients of the droop control and inertia control. These values are selected to maximize the inertial frequency. Δf_{WPP} is the frequency modulation, and it is calculated by the local measurement of the wind turbines.

2.3. Modelling f STATCOM

The output voltage of the STATCOM measured across the d and q axis are expressed in per unit (pu) as follows [55]:

$$v_{qSTAT} = V_{dSTAT} \times km_{STAT} \times \cos(\theta_{bus} + \alpha_{STAT}) \tag{10}$$

$$v_{dSTAT} = V_{dSTAT} \times km_{STAT} \times \sin(\theta_{bus} + \alpha_{STAT}) \tag{11}$$

where v_{qSTAT} and v_{dSTAT} represent the voltages at the q and d axis output terminals, respectively; α_{STAT} and k_{mSTAT} represents the STATCOM's phase angle and modulation index, respectively; and θ_{bus} denotes the phase angle of voltage across the common bus. The relation between current and voltage in the DC capacitor of STATCOM is given as follows [55]:

$$(C_m)_p (V_{dc\ STAT}) = \omega_b \left[I_{dc\ STAT} - \frac{V_{dc\ STAT}}{R_m} \right] \tag{12}$$

and here, p is presented as differential operator, which changes with time t and is determined by combining Equations (10) and (11) as follows [55]:

$$I_{dc\ STAT} = i_{q\ STAT} \times k_{m\ STAT} \times \cos(\theta_{bus} + \alpha_{STAT}) + i_{d\ STAT} \times k_{m\ STAT} \times \sin(\theta_{bus} + \alpha_{STAT}) \tag{13}$$

where I_{dcSTAT} indicates the DC current in pu, which passes through the positive end of DC voltage of the STATCOM, and R_m represents the equivalent resistance of the STATCOM. After implementing RSC, the DC voltage across the STATCOM is regulated by modifying the phase angle α_{STAT}, and the AC voltage is governed by varying k_{mSTAT}.

2.4. HVDC Rectifier Model

A power electronic converter is used for connecting the OWF-HVDC system with the onshore grid system. A fast-switching IGBT is used as a switching device for the rectifier. The DC voltage equation for the converter is given as follows [55]:

$$\frac{di_{rd}}{dt} = -\frac{R_r}{L_r}i_{rd} + \frac{1}{L_r}V_{Bd} - \frac{1}{L_r}V_{rd} + \omega i_{rq} \tag{14}$$

$$\frac{di_{rq}}{dt} = -\frac{R_r}{L_r}i_{rq} + \frac{1}{L_r}V_{Bq} - \frac{1}{L_r}V_{rq} + \omega i_{rd} \tag{15}$$

$$\frac{dV_{dcr}}{dt} = \frac{V_{Bd}i_{rd} + V_{Bq}i_{rq} - R_r\left(i^2_{rd} + i^2_{rq}\right)}{C_{dcr}V_{dcr}} - \frac{(V_{dcr} - V_{dci})}{C_{dcr}R_{dc}} \tag{16}$$

where R_{st} presents the resistance and L_{st} indicates reactance of the transformer in the rectifier; C_{dcr} and R_{dc} are defined as the capacitance and resistance of the DC link of HVDC; and V_{dcr} represents the voltage at the DC connection of the HVDC system.

When the currents flowing through the d-q axis are considered, regardless of the resistance of the stator, the following equations are used to calculate the active and reactive power of the stator in terms of the rotor current [53,54]:

$$\begin{cases} P_s = -\frac{L_m V_s}{L_s} \, i_{qrw} \\ Q_s = \frac{v_s^2}{\omega_s L_s} - \frac{L_m v_s}{L_s} i_{drw} \end{cases} \tag{17}$$

where P_s is active power, Q_s is reactive power, ω_s is the speed of the stator, v_s is the stator voltage, and L_s is the reactance of the stator.

3. Proposed Control Strategy of Hybrid LCVSC-HVDC System

A dynamic coordination control technique is implemented for the OWFs and power converters to achieve desired performance in terms of energy generation. In this research, the LCVSC is utilized for regulating the AC voltage and the frequency across the offshore. Here, the VSC is assumed as an ideal AC power supply, which can effectively absorb the generated wind energy. The schematic structure of the proposed hybrid multi-terminal HVDC system with LCVSC is demonstrated in Figure 1.
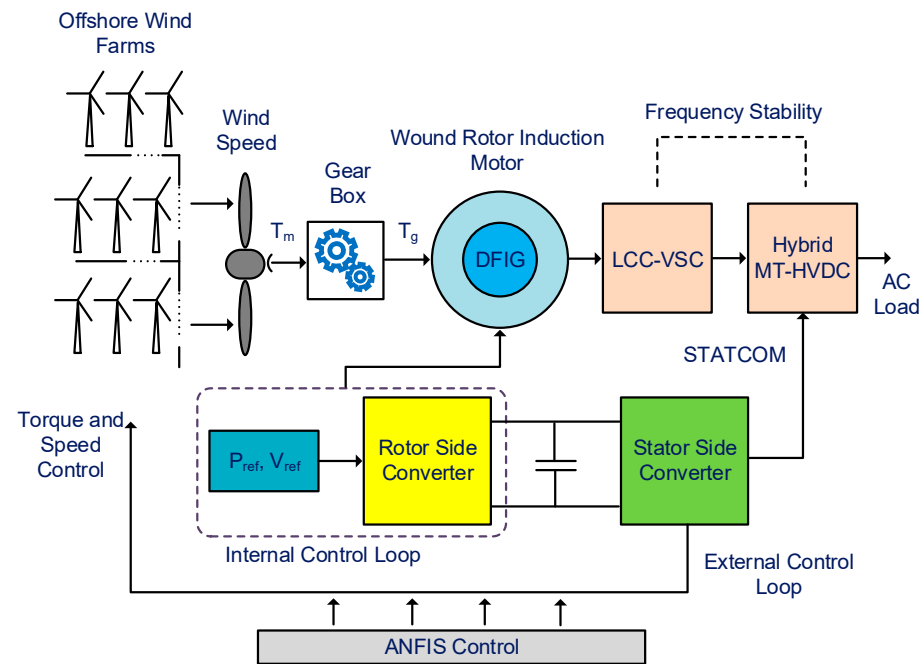

Figure 1. Schematic layout of the LCVSC-HVDC system.

The energy produced by the OWF is provided as an input to the wind turbine, which is linked to the DFIG through gearbox, as illustrated in Figure 1. The speed of the rotor is controlled by the DFIG, and the gearbox maintains the rotor speed and is synchronous with the speed of the DFIG. The hybrid MTDC system with the LCC and the VSC controller stabilizes the frequency of the MTDC. The transient stability is maintained using a STATCOM, which is connected between the AC load and the DFIG. The speed and frequency of the system varies throughout the operation in order to control the speed of the DFIG. The mechanical torque (T_m), generator torque (T_g), and reference signals (P_{ref} and V_{ref}) drive and control the operation of DFIG. A coordination control strategy combines Line Commutated Converter (LCC) and Voltage Source Converter (VSC) systems for enhancing the frequency stability of hybrid Multi-Terminal HVDC systems. The proposed control strategy utilizes the strengths of both LCVSC systems by combining them in a hybrid MTDC system. The primary objective of the proposed coordination control strategy is to address the frequency stability issues, which may arise due to the integration of renewable energy sources into the power grid. The flowchart represented in Figure 2 demonstrates the study process of

the control strategy for a hybrid Multi-Terminal HVDC system, which combines the LCC and the VSC controllers in order to stabilize frequency.
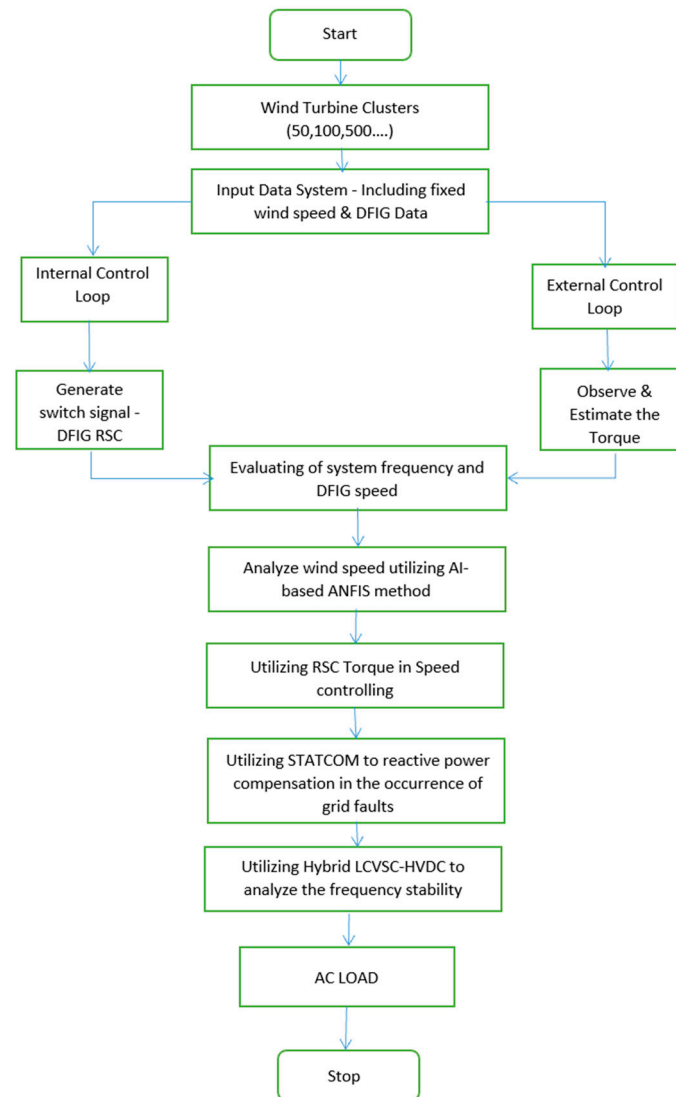

Figure 2. Flow chart of the control strategy of hybrid LCVSC-HVDC system.

3.1. Inner and External Control Loop

An inner and outer control loop are included in the proposed control approach in order to estimate the frequency and the voltage control of the DFIG and to obtain the adequate switching (reference) signals for the HVDC, the DFIG, and the VSC. The internal control loop is designed to generate appropriate switching signals for the RSC in DFIG, for the HVDC and for the STATCOM inverter.

The equations of the internal control loop are defined below as [55]:

$$X(t) = f(x) + g_u(x)u(t) \qquad (18)$$

$$y = h(x) \qquad (19)$$

The state of the system, input, and vectors for Equation (17) are given as follows [55]:

$$X = \begin{bmatrix} i_{d\ STAT}, & i_{q\ STAT}, & i_{rd}, & i_{rq}, & V_{dcr}, & i_{drw}, i_{qrw} \end{bmatrix} \qquad (20)$$

$$u = \left[V_{dst}, \; V_{qst}, V_{dr}, \; V_{qr}, \; V_{drw}, \; V_{qrw} \right] \tag{21}$$

$$y = \left[i_{d\,STAT}, \; i_{q\,STAT}, \; i_{dr}, \; V_{dcr}, \; P_s, \; Q_s \right] \tag{22}$$

The external loop is designed to control and determine the torque and to control the speed of the wind turbine, which represents the operation of the mechanical part of the turbine. The nonlinear equations defining the external control loop is given as follows [55]:

$$X(t) = f(x) + g_u(x)\,u(t) + gT(x)e(t) \tag{23}$$

$$y = h(x) \tag{24}$$

3.2. ANFIS Controller for Wind Speed Forecasting

Optimal use of the available wind resources is achieved with accurate wind speed forecasts, which improves power output projections. By assuring a more stable and predictable power supply from offshore wind farms, this in turn may help to maintain frequency stability. Superior performance is provided by the adaptive Neuro-Fuzzy Inference System (ANFIS) based regulating approach in terms of both predicting wind speed and maximizing power output. The ANFIS model, also known as the Adaptive Neuro-Fuzzy Inference System, is a model that combines the concepts of artificial neural networks (ANN) with the Fuzzy Inference System (FIS). The operating principle of the FIS of the ANFIS works follows a set of fuzzy IF-THEN rules, and it has a learning potential that can evaluate nonlinear systems. The ANFIS in this work tunes the control parameters of the DFIG, and the ANN in the ANFIS will provide an accurate prediction of wind speed. If 'p' and 'q' are the inputs and 'f' is the output of the ANFIS, the output of the first order FIS with two IF-THEN rules is given as follows:

Axiom 1: IF 'p' is X_1 & 'q' is Y_1; THEN $f_1 = a_1x + b_1y + z_1$
Axiom 2: IF 'p' is X_2 & 'q' is Y_2; THEN $f_2 = a_2x + b_2y + z_2$

Here, the terms a, b, and z are defined as the parameters for the first-order differential equations, which are updated continuously during the learning process. The architecture of the ANFIS controller is presented in Figure 3.
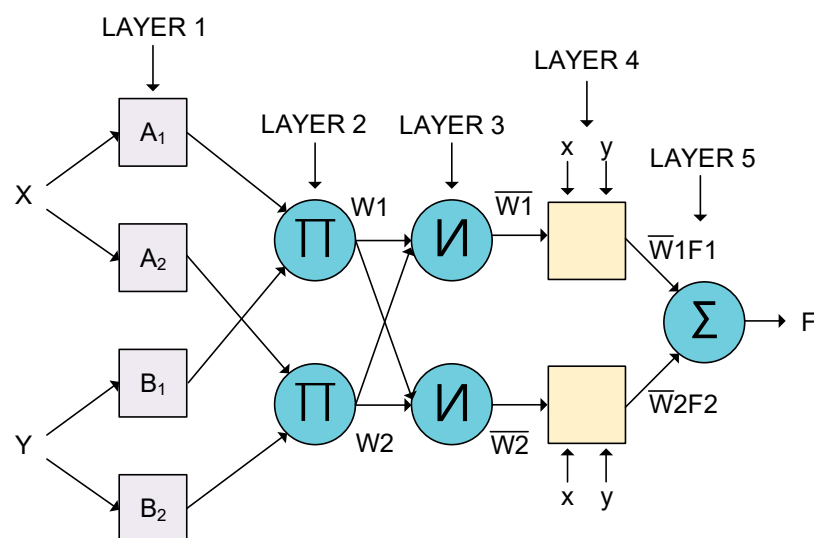

Figure 3. Architecture of ANFIS controller.

The architecture of the ANFIS possess five layers. The initial layer performs fuzzification wherein it selects the membership functions (MF) based on the given input. The second layer generates the rules for generating the firing strength. The third layer normalizes the

firing strength and the normalized strengths are fed as input to the fourth layer, which returns the values by performing defuzzification. The returned values are accepted by the fifth layer, which generates the final output. The membership function of the fuzzy logic controller lies between 0 and 1, and it is mathematically evaluated, as shown in the equation below [48]:

$$\mu P_j(x) = \frac{1}{1 + [((x - r_j)P_j^{-1})^2]^{b_j^{-3}}} \tag{25}$$

$$\mu P_j(x) = \exp[-[(\frac{x - r_j}{P_j})^2]^{b_j} \tag{26}$$

where P_j, r_j, and b_j are defined as the membership function parameters.

The parameters of the FIS are optimized using a back propagation technique, and the tuned parameter values are converted into fuzzy values depending on the membership functions and respective parametric values. Four main parameters, such as the base, inference engine, fuzzification, and defuzzification, are used in the design of the FIS. The design parameters of the FIS have a direct impact on the fuzzy inference systems. The membership functions of the FIS are decided using a trial-and-error approach, and the value of these functions is between 0 and 1. The following sections address both the effectiveness of the suggested control approach and the findings of the simulation analysis.

4. Results and Discussion

4.1. Experimental Details and System Configuration

An asynchronous DFIG model is modeled and simulated in this paper. The coordination control strategy that combines LCC and VSC enhancing frequency stability of hybrid HVDC (MTDC) systems is implemented in the Simulink. The proposed model is illustrated in Figure 4, and the parameters used in the design of DFIG are demonstrated in Table 1.
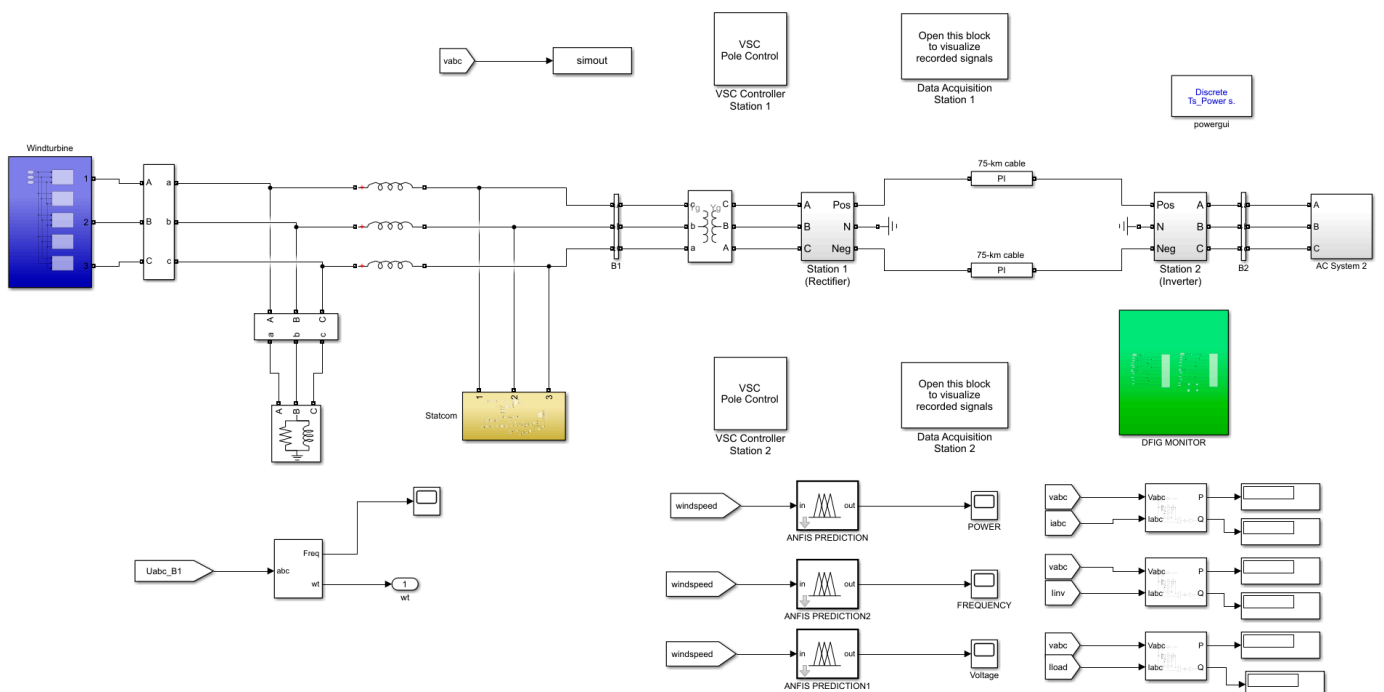

Figure 4. Simulink model of the proposed system.

Table 1. Modeling parameters for the DFIG.

Modeling Parameter	Values
Operating Frequency (f)	50 Hz
Speed of the rotor (N)	1500
Input voltage (V_s)	415 V
Stator Current (I_s)	1760 mA
Electromagnetic Torque (T_{em})	12,732 N
No of Poles	2
Rotor Voltage (V_r)	2070 V
Stator Resistance (R_s)	2.6×10^{-3} Ω
Stator Inductance (L_s)	0.087×10^{-3} H
Mutual Inductance (L_m)	2.5×10^{-3} H
Rotor Resistance (R_r)	2.9×10^{-3} Ω
Bus Voltage (V_{bus})	1150 V
Switching Frequency (f_{sw})	4×10^3 Hz
Switching Period (T_s)	0.25 ms

A high voltage and high current switching device IGBT are considered to achieve fast switching of the power electronic converter. To reduce the high voltage spikes across the load in a three-level bridge converter, a series of RC snubber circuits are placed in parallel with every switching device. The snubber resistance (R_s) and snubber capacitance are selected as 5000 Ω and 1×10^{-6} F, respectively.

4.2. Simulation Results

The simulation results of the RSC with respect to rotor speed, torque, Vs, i_{qr}, i_{dr}, I_s, V_{dr_ref}, V_{gr_ref}, and I_r are discussed in the figures below. The time period of the simulation is t = 10 s. The simulation results demonstrate the stability of the system when the wind turbine rotor speed rises from 7.5 rpm to 10 rpm at t = 3 s, and the corresponding changes in the RSC parameters can be observed in Figure 5.

Figure 5a–c present the transient responses of rotor speed, torque, and stator voltage, respectively. The transient response of the abovementioned parameters demonstrate that the system attains the stability after the changes occur in the rotor speed. Moreover, Figure 5d–i exhibit the transient responses of the rotor q-axis current, the rotor d-axis current, the stator current, the rotor d-axis voltage, the rotor q-axis voltage, and the roto current, respectively. These parameters all show a transient rise, and they subsequently move toward stability.

It can be observed from Figure 5 that all of the parameters mentioned in the text above swiftly attain the stable condition when the disturbance occurs, and hence improve the overall performance of the system.

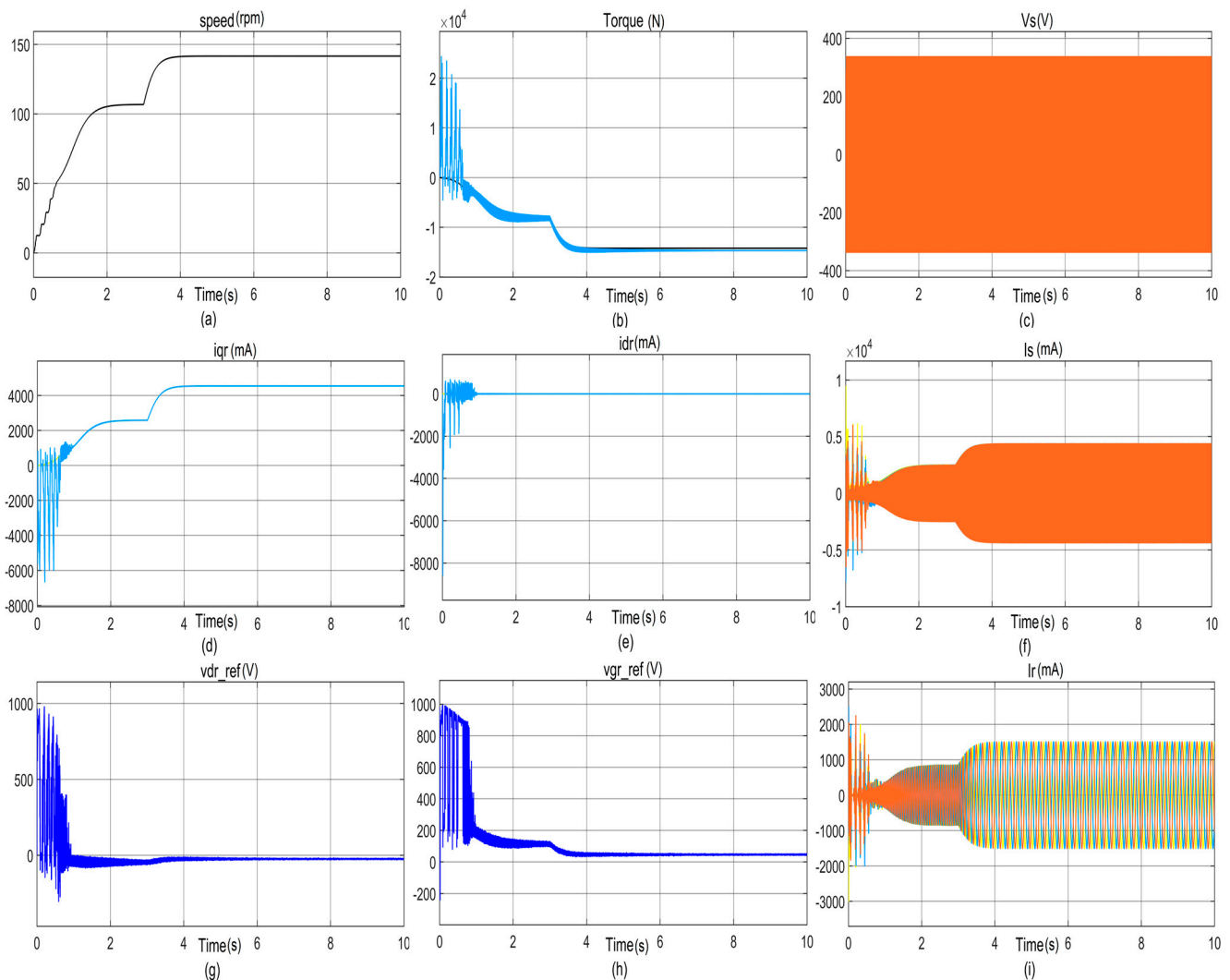The grid side output is illustrated in Figure 6.

Figure 5. Simulation results of the output of RSC.

From Figure 6, it is also clear that when the disturbance occurs, the various system parameters of grid side also acquire stability in a very short amount of time.

Additionally, the transient behaviors of bus voltage, reactive power, and stator voltage on the grid side are depicted by the Figure 6a–c respectively. As the rotor speed varies, these parameters acquire stability, as presented in the Figure 6. Figure 6d–i present the transient responses of the grid side converter d-axis current, the grid side converter q-axis current, the grid converter current, the grid side converter d-axis voltage, the grid side converter q-axis voltage, and the active power generated, respectively. A transient increment happens as the rotor speed varies, and, finally, all of these parameters show stability.

The frequency stability using the proposed controller approach is shown in Figure 7. It can be observed from Figure 7 that regardless of initial disturbances, the frequency attains a constant state soon after a specific amount of time. The stability of the waveform depicting the variation in the frequency can be observed after 1–2 s of time.
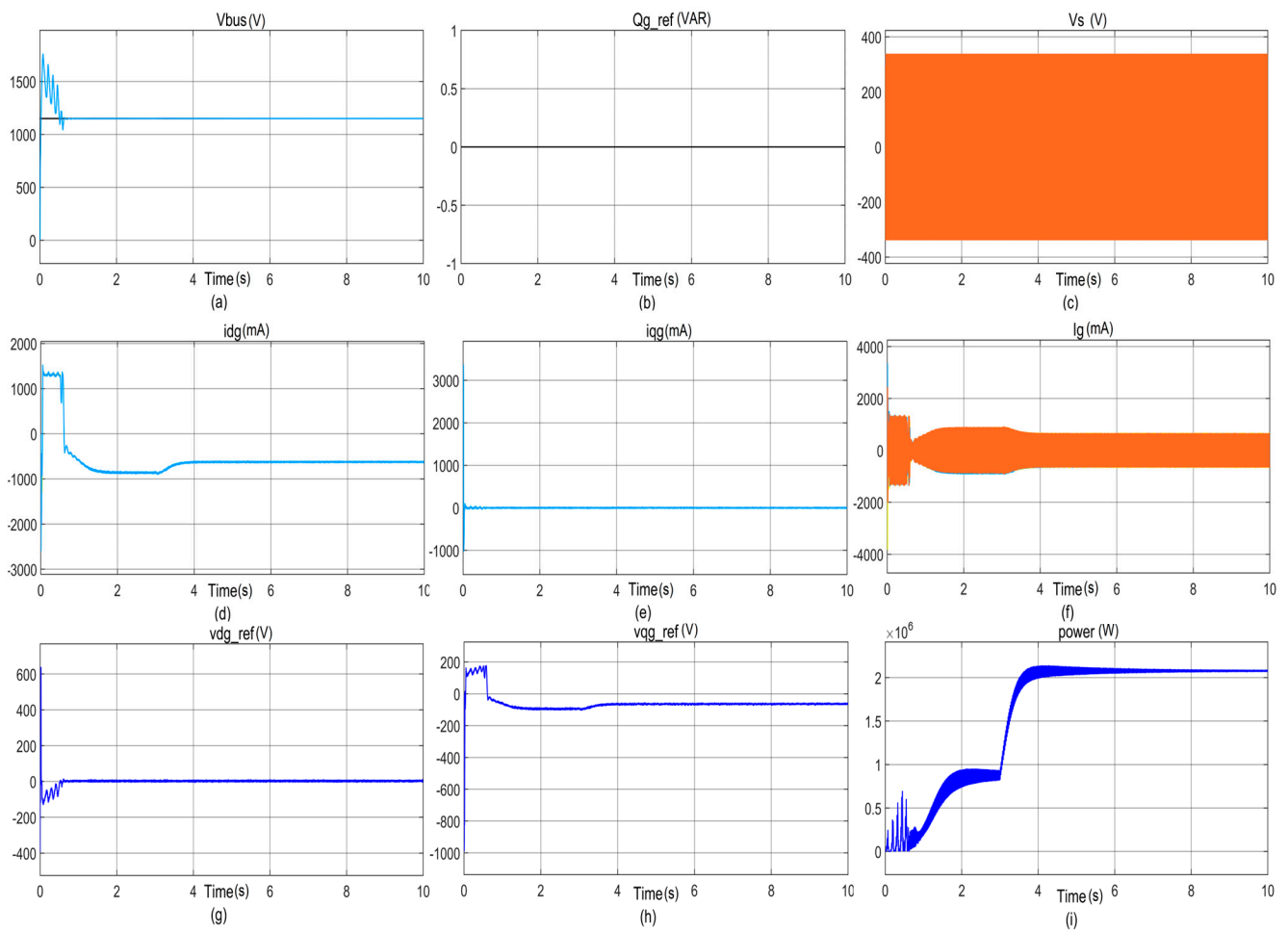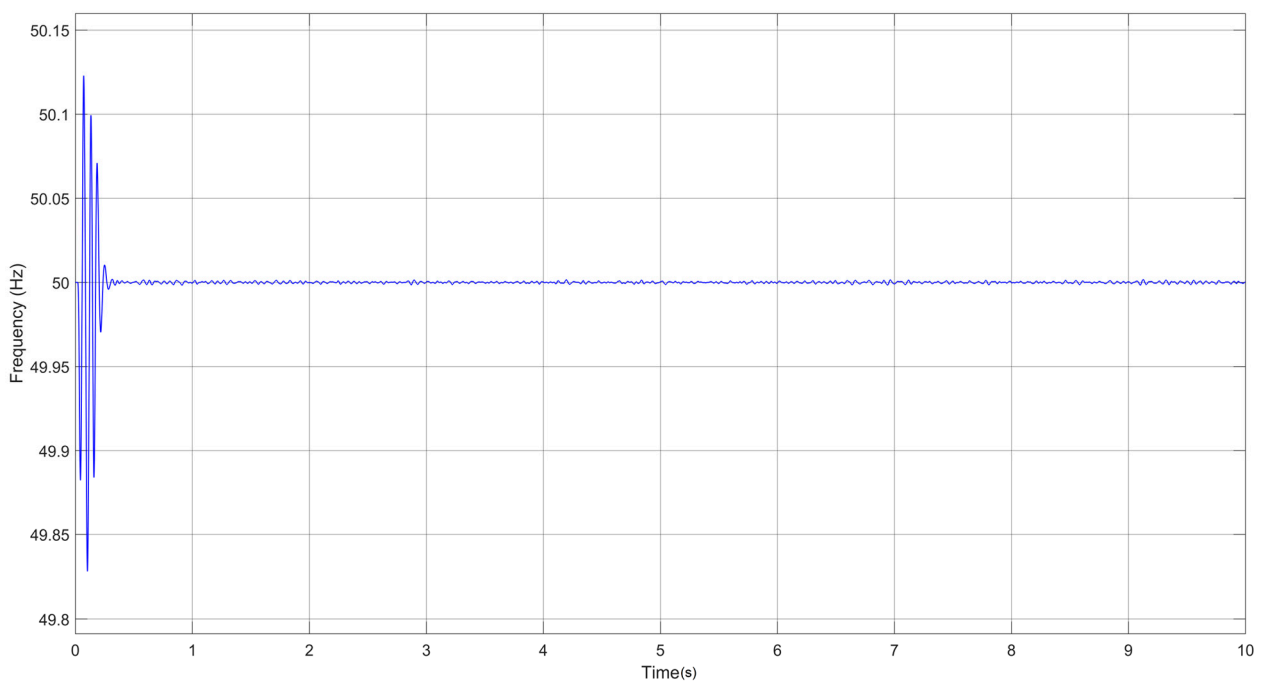
Figure 6. Grid side output.

Figure 7. Frequency stability using proposed control approach.

The output of converter is DC side on offshore and travels 100 km, and LCC is used in HVDC for bulk power transmission over long distances. On the other hand, VSC-based HVDC is also a solution for long-distance power transmission, especially for off-shore wind plants and for supplying power to remote regions.

The proposed LCVSC-HVDC is connected with a 12 pulse three-level bridge converter, which transfers power from one end to another end with a 1000 km long cable. STATCOM is implemented using power inverters for injecting the reactive power whenever it is required by the system. STATCOM improves the transient stability of the system, which can be observed in Figure 8 below:
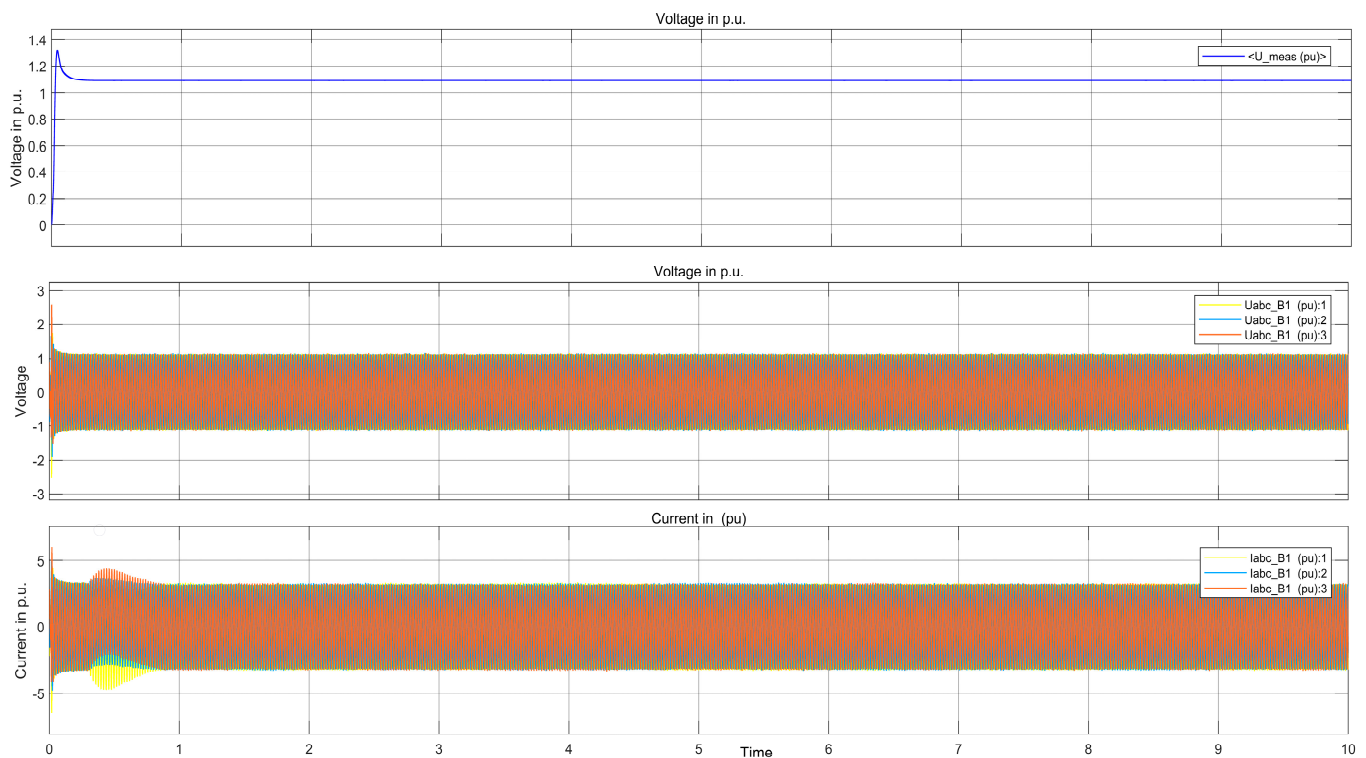
Figure 8. Output of voltage and current across STATCOM.

Figure 9 shows an illustration of the change in wind speed over time. Based on the findings of the simulations, it can be deduced that the system control technique is useful in lowering the levels of system disturbances. The stability in wind speed and power output can be observed after the initial set-up time. The adaptive Neuro-Fuzzy Inference System (ANFIS) based controlling technique offers superior performance in both forecasting wind speed and maximizing power generation. Accurate wind speed forecasting leads to better power output predictions and to optimal utilization of available wind resources. In turn, this contributes to frequency stability by ensuring a more consistent and reliable power supply from offshore wind farms. The performance of the ANFIS in terms of forecasting the frequency, power, and voltage at various speeds is shown in Figures 10–12 accordingly, which are presented below.
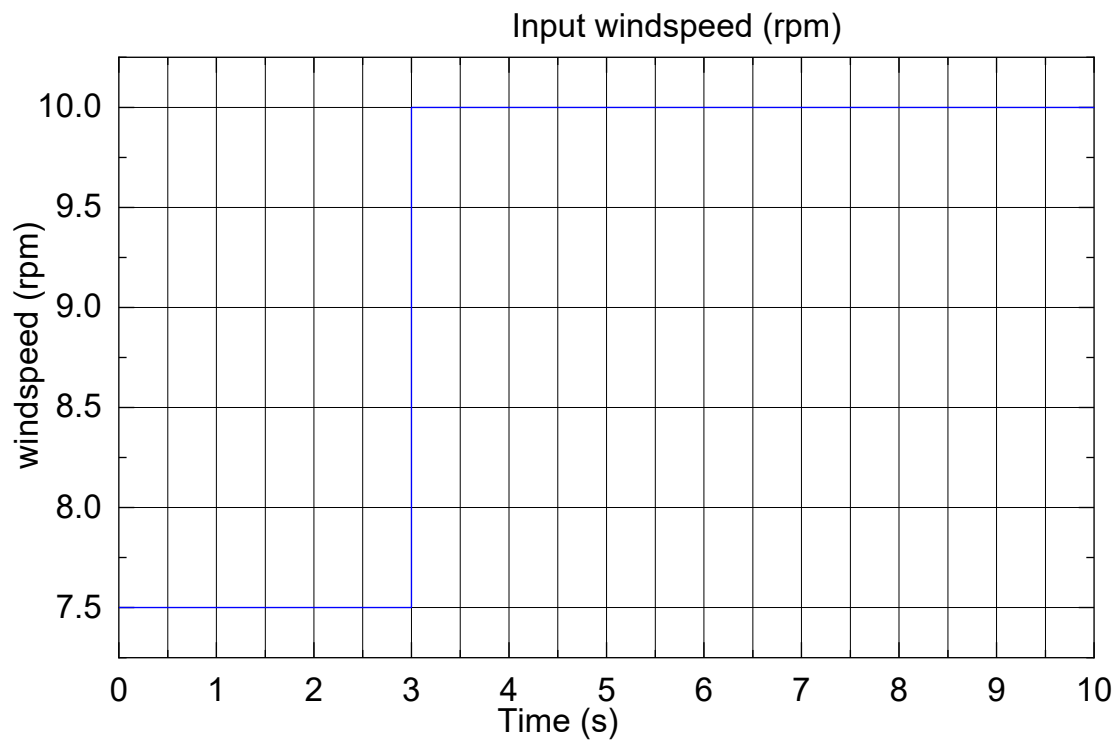
Input windspeed (rpm)

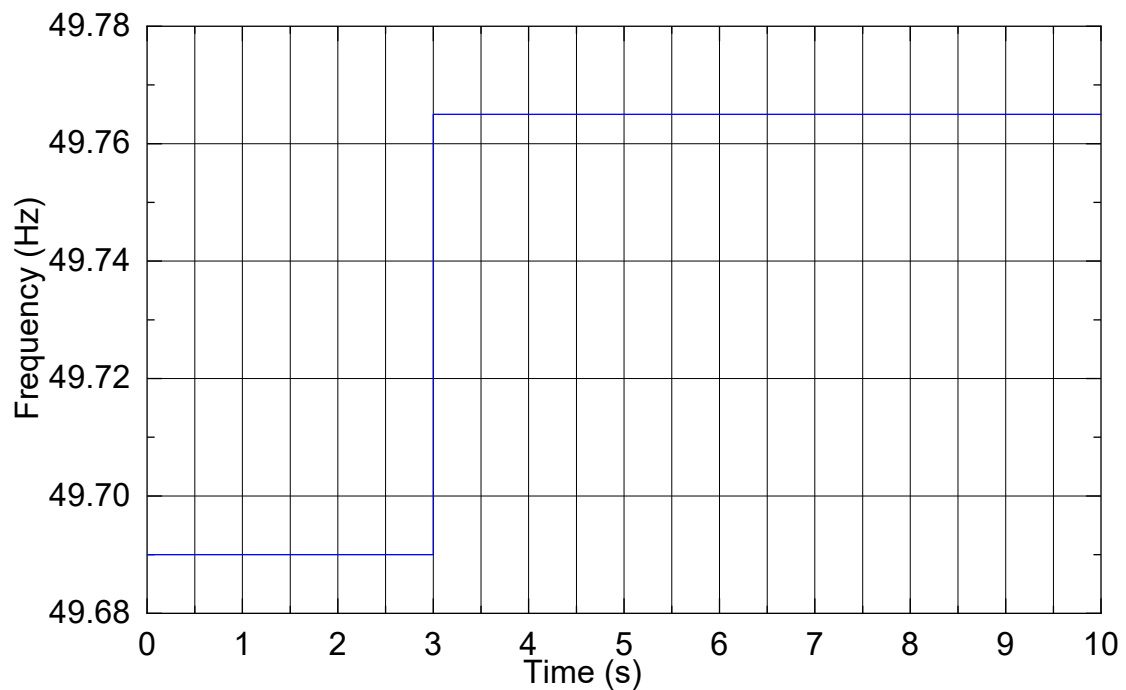**Figure 9.** Variation in the wind speed with respect to time.

Figure 10. Frequency prediction using ANFIS.

These predictions are measured by using the oscilloscope meters, as shown in the Simulink model of Figure 4. As the wind speed varies, the adaptive Neuro-Fuzzy Inference System (ANFIS) based controller accurately predicts the frequency, power, and voltage.

The stability of the wind speed and power validates the performance of the suggested control technique. Here, the reactive power of the inverter is equal to the reactive power of load (i.e., $Q_{inv} = Q_{load}$) with different AC loads connected with each other.
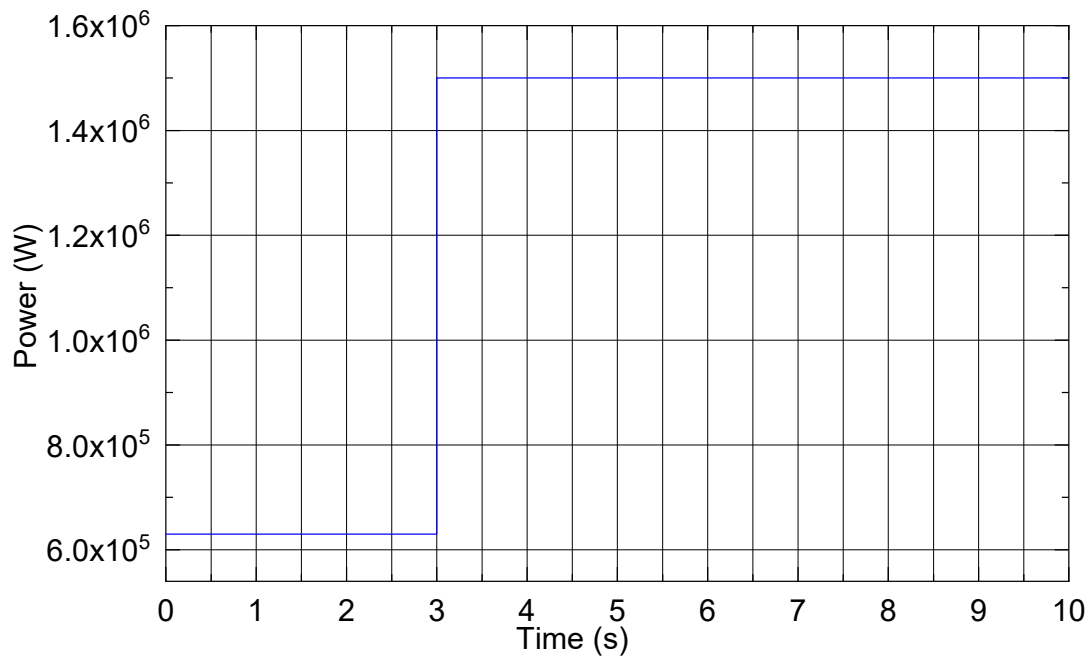
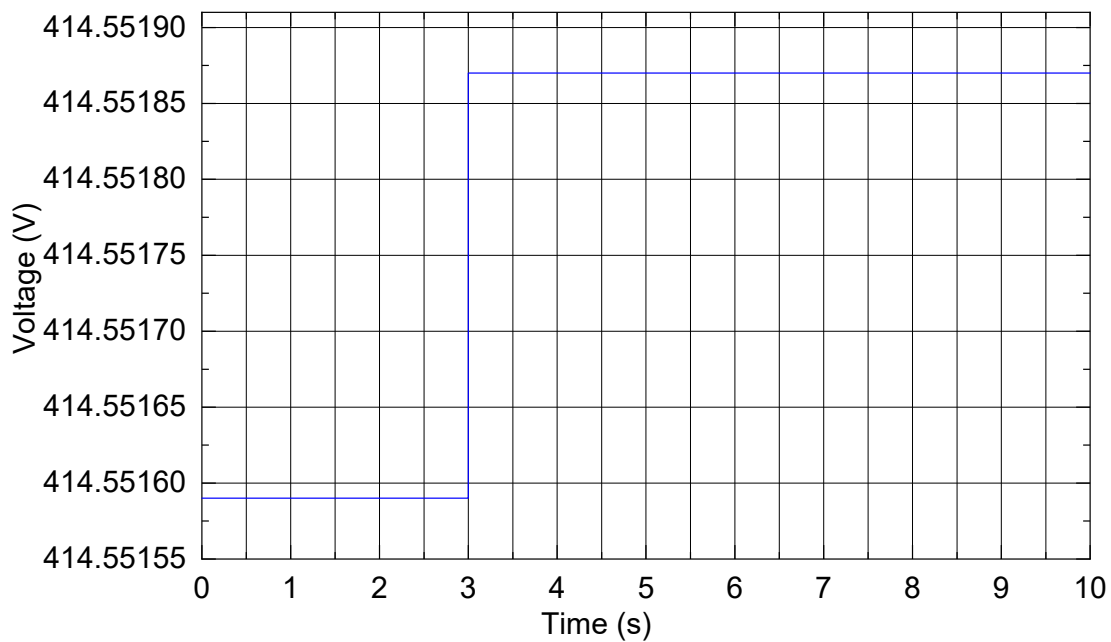**Figure 11.** Power prediction using ANFIS.

Figure 12. Voltage prediction using ANFIS.

4.3. Comparative Analysis

The proposed system was evaluated based on various parameters to assess its performance. These parameters included frequency, wind power, rotor and stator side current, torque, speed, and power. During the simulation in MATLAB/SIMULINK, these parameters were carefully measured in order to ensure accurate performance evaluation. The experimental set-up used to validate the performance of the proposed approach was compared with the conventional optimal power flow (OPF) model. This comparison approach was evaluated under different operating conditions, including varying wind speeds and power outputs. The performance of the proposed enhanced frequency optimal power flow (EFOPF) is compared with the conventional OPF method, and the results of the comparative analysis is discussed in the simulation graphs shown below. The simulation is conducted

for two different conditions: the maximum frequency is 50.5 Hz (f_{max}) and the minimum frequency is 49.5 Hz (f_{min}).

The frequency fluctuations that are depicted in Figures 13 and 14 demonstrate that the existing OPF offers a solution that pushes the frequency nadirs of the two grid systems beyond the permissible contingency bands for various time periods, and this is demonstrated by the fact that the solution is provided by the Figures. However, the suggested EFOPF solves this issue by utilizing a dynamic coordination control technique for HVDC systems, and, as a result, it is able to attain superior performance in comparison to the OPF method that is currently in use.
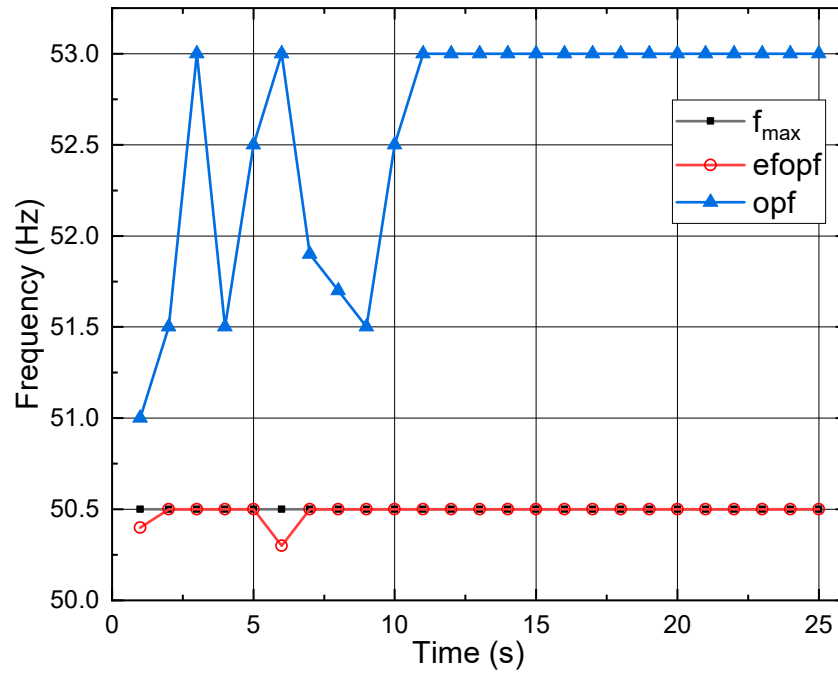
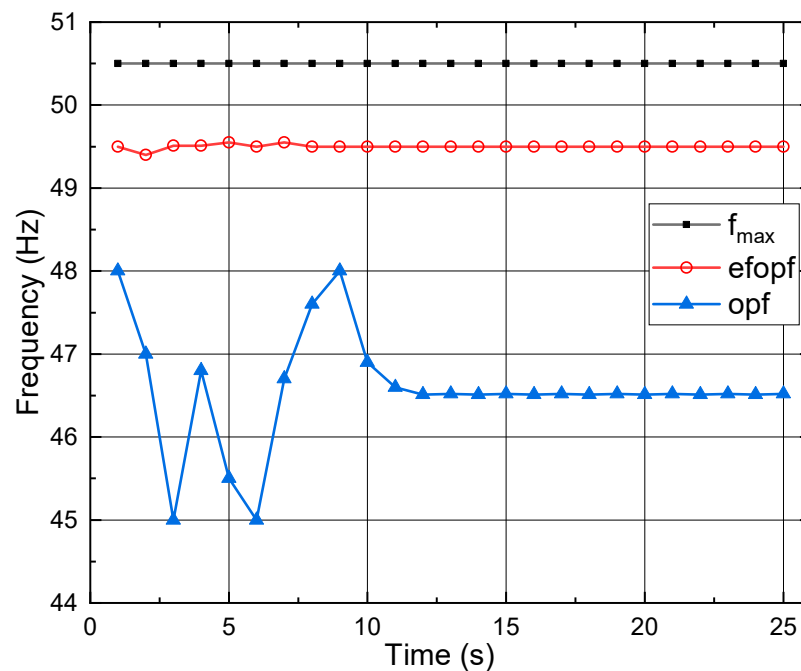**Figure 13.** Variation in frequency of HVDC at f_{max} = 50.5 Hz.

Figure 14. Variation in frequency of HVDC at f_{max} = 49.2 Hz.

5. Conclusions

A novel controlling approach was suggested for stabilizing the frequency of the multi-terminal HVDC systems connected with a DFIG-based OWFs. The proposed dynamic control strategy incorporated both the LCC and the VSC to enable bulk transmission of power over long distances. The regulated voltage and power allow large-scale power transmission using the proposed HVDC system. Simulation analysis was used to evaluate the effectiveness of the newly established approach, wherein the model was simulated with respect to different parameters, such as wind speed, variation in frequency, and grid side and rotor side voltage. By implementing an ANFIS controller to predict the wind speed, the dynamic performance of the HVDC system was enhanced. According to the findings, the suggested method delivered superior frequency stability performance in comparison to the existing technique. In future, this research intends to explore different frequency control strategies for asynchronous AC grids based on artificial intelligence-based methods to handle over- and under-frequency disturbances.

Abbreviations

DFIG	Double Fed Induction Generator
AC	Alternating current
DC	Direct current
HVAC	High voltage alternating Current
HVDC	High voltage direct current
LCC	Line-commutated converters
VSC	Voltage Source Converters
MTDC	Multi-terminal direct current
HMTDC	Hybrid multi-terminal direct current
RSC	Rotor side controller
GSC	Gird side controller
OPF	Optimal power flow
OWFs	Offshore wind farms
GW	Gigawatt
MW	Megawatt
ANFIS	Adaptive Neuro-Fuzzy Inference System
WTs	Wind turbines
EFOPF	Enhanced frequency optimal power flow
MT-HVDC	Multi terminal high voltage direct current
LCVSC	Line-commutated voltage source converters

References

1. Li, C.; Zhan, P.; Wen, J.; Yao, M.; Li, N.; Lee, W.J. Offshore wind farm integration and frequency support control utilizing hybrid multiterminal HVDC transmission. *IEEE Trans. Ind. Appl.* **2013**, *50*, 2788–2797. [CrossRef]
2. Breyer, C.; Khalili, S.; Bogdanov, D.; Ram, M.; Oyewo, A.S.; Aghahosseini, A.; Gulagi, A.; Solomon, A.A.; Keiner, D.; Lopez, G.; et al. On the History and Future of 100% Renewable Energy Systems Research. *IEEE Access* **2022**, *10*, 78176–78218. [CrossRef]
3. Chang, Y.; Zhao, M.; Kocar, I. The impact of DFIG control schemes on the negative-sequence based differential protection. *Electr. Power Syst. Res.* **2022**, *211*, 108564. [CrossRef]
4. Chang, Y.; Mahseredjian, J.; Kocar, I.; Karaagac, U. Analytical characterization of DFIG response to asymmetrical voltage dips for efficient design. *Electr. Power Syst. Res.* **2022**, *211*, 108553. [CrossRef]
5. Musial, W.D. *Large-Scale Offshore Wind Power in the United States*; National Renewable Energy Laboratory: Golden, CO, USA, 2010.
6. Chen, Y.; Bhutta, M.S.; Abubakar, M.; Xiao, D.; Almasoudi, F.M.; Naeem, H.; Faheem, M. Evaluation of Machine Learning Models for Smart Grid Parameters: Performance Analysis of ARIMA and Bi-LSTM. *Sustainability* **2023**, *15*, 8555. [CrossRef]
7. Zhou, W.; Li, Q.; Wu, K.; Zhang, L.; Hassan, M.A.S.; Chen, M. Accelerated hierarchical optimization method for emergency energy management of microgrids with energy storage systems. *Energy Sci. Eng.* **2022**, *10*, 962–972. [CrossRef]
8. Chen, W.; Liu, B.; Nazir, M.S.; Abdalla, A.N.; Mohamed, M.A.; Ding, Z.; Bhutta, M.S.; Gul, M. An energy storage assessment: Using frequency modulation approach to capture optimal coordination. *Sustainability* **2022**, *14*, 8510. [CrossRef]
9. Van Eeckhout, B.; Van Hertem, D.; Reza, M.; Srivastava, K.; Belmans, R. Economic comparison of VSC HVDC and HVAC as transmission system for a 300 MW offshore wind farm. *Eur. Trans. Electr. Power* **2010**, *20*, 661–671. [CrossRef]
10. Rahman, S.; Khan, I.; Alkhammash, H.I.; Nadeem, M.F. A comparison review on transmission mode for onshore integration of offshore wind farms: Hvdc or hvac. *Electronics* **2021**, *10*, 1489. [CrossRef]
11. Guo, Y.; Gao, H.; Xing, H.; Wu, Q.; Lin, Z. Decentralized coordinated voltage control for VSC-HVDC connected wind farms based on ADMM. *IEEE Trans. Sustain. Energy* **2018**, *10*, 800–810. [CrossRef]
12. Lu, Z.; Ye, Y.; Qiao, Y. An adaptive frequency regulation method with grid-friendly restoration for VSC-HVDC integrated offshore wind farms. *IEEE Trans. Power Syst.* **2019**, *34*, 3582–3593. [CrossRef]
13. Lee, G.; Moon, S.; Hwang, P. A Frequency–Power Droop Coefficient Determination Method of Mixed Line-Commutated and Voltage-Sourced Converter Multi-Infeed, High-Voltage, Direct Current Systems: An Actual Case Study in Korea. *Appl. Sci.* **2019**, *9*, 606. [CrossRef]
14. Yamashita, K.I.; Tsukamoto, G.; Nishikata, S. Steady-state characteristics of a line-commutated converter-based high-voltage direct current transmission system for series-connected wind power plants. *IEEE Trans. Ind. Appl.* **2020**, *56*, 3932–3939. [CrossRef]
15. Zhan, P.; Li, C.; Wen, J.; Hua, Y.; Yao, M.; Li, N. Research on hybrid multi-terminal high-voltage DC technology for offshore wind farm integration. *J. Mod. Power Syst. Clean Energy* **2013**, *1*, 34–41. [CrossRef]
16. Haleem, N.M.; Rajapakse, A.D.; Gole, A.M.; Fernando, I.T. Investigation of fault ride-through capability of hybrid VSC-LCC multi-terminal HVDC transmission systems. *IEEE Trans. Power Deliv.* **2018**, *34*, 241–250. [CrossRef]
17. Li, M.; Yang, M.; Yu, Y.; Lee, W.J. A wind speed correction method based on modified hidden Markov model for enhancing wind power forecast. *IEEE Trans. Ind. Appl.* **2021**, *58*, 656–666. [CrossRef]
18. Liao, K.; Pang, B.; Yang, J.; He, Z. Compensation Strategy of Wideband Voltage Harmonics for Doubly-Fed Induction Generator. *IEEE Trans. Energy Convers.* **2023**, *38*, 674–684. [CrossRef]
19. Liao, K.; Lu, D.; Wang, M.; Yang, J. A Low-Pass Virtual Filter for Output Power Smoothing of Wind Energy Conversion Systems. *IEEE Trans. Ind. Electron.* **2022**, *69*, 12874–12885. [CrossRef]
20. Liang, J.; Kato, B.; Wang, Y. Constructing simplified models for dynamic analysis of monopile-supported offshore wind turbines. *Ocean Eng.* **2023**, *271*, 113785. [CrossRef]
21. Guo, C.; Hu, J. Fixed-Time Stabilization of High-Order Uncertain Nonlinear Systems: Output Feedback Control Design and Settling Time Analysis. *J. Syst. Sci. Complex.* **2023**. [CrossRef]
22. Pan, W.; Chang, Y.; Chen, H. Hybrid multi-terminal HVDC system for large scale wind power. In Proceedings of the 2006 IEEE PES Power Systems Conference and Exposition, Atlanta, GA, USA, 29 October–1 November 2006; pp. 755–759.
23. Chen, X.; Sun, H.; Wen, J.; Lee, W.J.; Yuan, X.; Li, N.; Yao, L. Integrating wind farm to the grid using hybrid multiterminal HVDC technology. *IEEE Trans. Ind. Appl.* **2010**, *47*, 965–972. [CrossRef]
24. Torres-Olguin, R.E.; Molinas, M.; Undeland, T. Offshore wind farm grid integration by VSC technology with LCC-based HVDC transmission. *IEEE Trans. Sustain. Energy* **2012**, *3*, 899–907. [CrossRef]
25. Faheem, M.; Umar, M.; Butt, R.A.; Raza, B.; Ngadi, M.A.; Gungor, V.C. Software defined communication framework for smart grid to meet energy demands in smart cities. In Proceedings of the 2019 7th International Istanbul Smart Grids and Cities Congress and Fair (ICSG), Istanbul, Turkey, 25–26 April 2019; pp. 51–55.
26. Faheem, M.; Fizza, G.; Ashraf, M.W.; Butt, R.A.; Ngadi, M.A.; Gungor, V.C. Big Data acquired by Internet of Things-enabled industrial multichannel wireless sensors networks for active monitoring and control in the smart grid Industry 4.0. *Data Brief* **2021**, *35*, 106854. [CrossRef] [PubMed]

27. Hassan, M.A.S.; Assad, U.; Farooq, U.; Kabir, A.; Khan, M.Z.; Bukhari, S.S.H.; Jaffri, Z.U.A.; Oláh, J.; Popp, J. Dynamic price-based demand response through linear regression for microgrids with renewable energy resources. *Energies* **2022**, *15*, 1385. [CrossRef]

28. Nazir, M.S.; Abdalla, A.N.; Zhao, H.; Chu, Z.; Nazir, H.M.J.; Bhutta, M.S.; Javed, M.S.; Sanjeevikumar, P. Optimized economic operation of energy storage integration using improved gravitational search algorithm and dual stage optimization. *J. Energy Storage* **2022**, *50*, 104591. [CrossRef]

29. Trevisan, A.S.; Fecteau, M.; Mendonça, Â.; Gagnon, R.; Mahseredjian, J. Analysis of low frequency interactions of DFIG wind turbine systems in series compensated grids. *Electr. Power Syst. Res.* **2021**, *191*, 106845. [CrossRef]

30. Camargo, R.S.; Amorim, A.E.A.; Bueno, E.J.; Encarnaçao, L.F. Novel multilevel STATCOM for power system stability enhancement on DFIG-based wind farms. *Electr. Power Syst. Res.* **2021**, *197*, 107316. [CrossRef]

31. Bhutta, M.S.; Sarfraz, M.; Ivascu, L.; Li, H.; Rasool, G.; ul Abidin Jaffri, Z.; Farooq, U.; Ali Shaikh, J.; Nazir, M.S. Voltage Stability Index Using New Single-Port Equivalent Based on Component Peculiarity and Sensitivity Persistence. *Processes* **2021**, *9*, 1849. [CrossRef]

32. Zhang, Y.; Klabunde, C.; Wolter, M. Study of resonance issues between DFIG-based offshore wind farm and HVDC transmission. *Electr. Power Syst. Res.* **2021**, *190*, 106767. [CrossRef]

33. Liu, H.; Sun, J. Voltage stability and control of offshore wind farms with AC collection and HVDC transmission. *IEEE J. Emerg. Sel. Top. Power Electron.* **2014**, *2*, 1181–1189.

34. Kunjumuhammed, L.P.; Pal, B.C.; Gupta, R.; Dyke, K.J. Stability analysis of a PMSG-based large offshore wind farm connected to a VSC-HVDC. *IEEE Trans. Energy Convers.* **2017**, *32*, 1166–1176. [CrossRef]

35. Zhou, W.; Wang, Y.; Torres-Olguin, R.E.; Chen, Z. Effect of reactive power characteristic of offshore wind power plant on low-frequency stability. *IEEE Trans. Energy Convers.* **2020**, *35*, 837–853. [CrossRef]

36. O'Sullivan, J.; Rogers, A.; Flynn, D.; Smith, P.; Mullane, A.; O'Malley, M. Studying the maximum instantaneous non-synchronous generation in an island system—Frequency stability challenges in Ireland. *IEEE Trans. Power Syst.* **2014**, *29*, 2943–2951. [CrossRef]

37. Chávez, H.; Baldick, R.; Sharma, S. Governor rate-constrained OPF for primary frequency control adequacy. *IEEE Trans. Power Syst.* **2014**, *29*, 1473–1480. [CrossRef]

38. Chvez, H.; Baldick, R.; Matevosyan, J. The joint adequacy of AGC and primary frequency response in single balancing authority systems. *IEEE Trans. Sustain. Energy* **2015**, *6*, 959–966. [CrossRef]

39. Dvorkin, Y.; Henneaux, P.; Kirschen, D.S.; Pandžić, H. Optimizing primary response in preventive security-constrained optimal power flow. *IEEE Syst. J.* **2016**, *12*, 414–423. [CrossRef]

40. Wen, Y.; Li, W.; Huang, G.; Liu, X. Frequency dynamics constrained unit commitment with battery energy storage. *IEEE Trans. Power Syst.* **2016**, *31*, 5115–5125. [CrossRef]

41. Carrasco, F.; Rahmann, C. Effects of inertial response and ramp reserve requirements in the unit commitment. In Proceedings of the 2016 IEEE Power and Energy Society General Meeting (PESGM), Boston, MA, USA, 17–21 July 2016; pp. 1–5.

42. Junyent-Ferr, A.; Pipelzadeh, Y.; Green, T.C. Blending HVDC-link energy storage and offshore wind turbine inertia for fast frequency response. *IEEE Trans. Sustain. Energy* **2014**, *6*, 1059–1066. [CrossRef]

43. Abu-Elanien, A.E.; Abdel-Khalik, A.S.; Massoud, A.M. Multi-terminal HVDC system with offshore wind farms under anomalous conditions: Stability assessment. *IEEE Access* **2021**, *9*, 92661–92675. [CrossRef]

44. Pinto, R.T.; Aragüés-Peñalba, M.; Gomis-Bellmunt, O.; Sumper, A. Optimal operation of DC networks to support power system outage management. *IEEE Trans. Smart Grid* **2016**, *7*, 2953–2961. [CrossRef]

45. Bernal-Perez, S.; Añó-Villalba, S.; Blasco-Gimenez, R. Stability analysis of multi-terminal HVDC with diode rectifier connected off-shore wind power plants. *Int. J. Electr. Power Energy Syst.* **2021**, *124*, 106231. [CrossRef]

46. Mehrabankhomartash, M.; Saeedifard, M.; Yazdani, A. Adjustable wind farm frequency support through multi-terminal HVDC grids. *IEEE Trans. Sustain. Energy* **2021**, *12*, 1461–1472. [CrossRef]

47. Rekik, A.; Boukettaya, G. A Dynamic Power Management and Dedicated Control Strategy of a Flexible Multi-Terminal HVDC Grids for Offshore Wind Farms. *Int. J. Renew. Energy Res.* **2021**, *11*, 247–263.

48. Yan, S.; Gu, Z.; Park, J.H.; Xie, X. Adaptive memory-event-triggered static output control of T–S fuzzy wind turbine systems. *IEEE Trans. Fuzzy Systems* **2021**, *30*, 3894–3904. [CrossRef]

49. Yan, S.; Gu, Z.; Park, J.H.; Xie, X. Synchronization of delayed fuzzy neural networks with probabilistic communication delay and its application to image encryption. *IEEE Trans. Fuzzy Syst.* **2022**, *31*, 930–940. [CrossRef]

50. Wen, Y.; Chung, C.Y.; Ye, X. Enhancing frequency stability of asynchronous grids interconnected with HVDC links. *IEEE Trans. Power Syst.* **2018**, *33*, 1800–1810. [CrossRef]

51. Huynh, N.T.; Nguyen, T.V.; Nguyen, Q.M. Optimum Design for the Magnification Mechanisms Employing Fuzzy Logic-ANFIS. *Comput. Mater. Contin.* **2022**, *73*, 5961–5983.

52. Nguyen, T.V.; Huynh, N.T.; Vu, N.C.; Kieu, V.N.; Huang, S.C. Optimizing compliant gripper mechanism design by employing an effective bi-algorithm: Fuzzy logic and ANFIS. *Microsyst. Technol.* **2021**, *27*, 3389–3412. [CrossRef]

53. Roungrojkarnranan, V.; Chen, X. Reactive Power Compensation and Energy Storage in Wind Power Plant. Bachelor's Thesis, Worcester Polytechnic Institute, Worcester, MA, USA, 2012.

54. Ahmad, R.; Abdul-Hussain, M. Modeling and simulation of wind turbine generator using Matlab-Simulink. *J. Al-Rafidain Univ. Coll. Sci.* **2017**, *40*, 282–300.

55. Dash, P.K.; Nayak, N. Nonlinear control of voltage source converters in AC–DC power system. *ISA Trans.* **2014**, *53*, 1268–1285. [CrossRef]